RSC Medicinal Chemistry

ROYAL SOCIETY OF CHEMISTRY

RESEARCH ARTICLE

View Article Online
View Journal | View Issue

Cite this: *RSC Med. Chem.*, 2020, **11**, 665

Understanding the mechanism of action of pyrrolo[3,2-*b*]quinoxaline-derivatives as kinase inhibitors†

Andrea Unzue,[a] Claudia Jessen-Trefzer,[a] Dimitrios Spiliotopoulos,[b] Eugenio Gaudio,[c] Chiara Tarantelli,[c] Jing Dong,[b] Hongtao Zhao,[b] Johanna Pachmayr,[d] Stefan Zahler,[d] Elena Bernasconi,[c] Giulio Sartori,[c] Luciano Cascione, [ce] Francesco Bertoni, [*cf] Paweł Śledź,[b] Amedeo Caflisch*[b] and Cristina Nevado [*a]

Received 12th February 2020,
Accepted 16th April 2020

DOI: 10.1039/d0md00049c

rsc.li/medchem

The X-ray structure of the catalytic domain of the EphA3 tyrosine kinase in complex with a previously reported type II inhibitor was used to design two novel quinoxaline derivatives, inspired by kinase inhibitors that have reached clinical development. These two new compounds were characterized by an array of cell-based assays and gene expression profiling experiments. A global chemical proteomics approach was used to generate the drug-protein interaction profile, which suggested suitable therapeutic indications. Both inhibitors, studied in the context of angiogenesis and *in vivo* in a relevant lymphoma model, showed high efficacy in the control of tumor size.

Introduction

Drug development is a risky and expensive process[1] in which only 8% of the candidates that enter clinical trials are approved by the authorities.[2] Late-stage failures of promising drug candidates in clinical development have emphasized the importance of understanding their mode of action.[2] As a result, more personalized treatments can be developed, new clinical applications of already approved drugs can be conceived, and a better understanding of off-target effects can be achieved. The application of systems biology approaches, including studies based on gene signatures that inform on pathways and diseases that the drug of interest acts on,[3] or chemical proteomics technology, where binding of the molecule of interest is addressed in an unbiased environment to obtain its global target profile, have proven efficient in this regard. In fact, such studies have been applied to several kinase inhibitors including dasatinib, imatinib, nilotinib[4] and bosutinib,[5] revealing clear differences in the mode of action of these drugs despite being all administered for the treatment of chronic myeloid leukemia (CML).

Protein kinases are relevant targets for the treatment of diseases including cancer, inflammation, cardiovascular conditions and immune-related disorders.[6] More than 50 small-molecule kinase inhibitors have been approved by the FDA over the last decade.[7] In our work, we have focused on the *in silico* design, synthesis and computational-aided optimization of potent and selective receptor tyrosine kinase inhibitors.[8] To date, our approach has yielded nanomolar EphB4 inhibitors whose binding modes, antiproliferative activities and *in vivo* efficacies have been characterized.[9]

Here we describe the design, synthesis and in depth biological characterization of the mode of action of two novel type II kinase inhibitors (**8a**, **b**) with broader scope of activity. The two compounds showed *in vivo* anti-tumor activity, especially in models derived from hematological malignancies. The effects of these molecules on gene expression were compared to dasatinib, an FDA approved drug for the treatment of chronic myeloid leukemia.[10] Further characterization, including the assessment of their *in vitro* selectivity, cellular angiogenesis inhibition, as well as a global chemical proteomics approach and *in vivo* efficacy is reported here.

[a] *Department of Chemistry, University of Zurich, Winterthurerstrasse 190, CH-8057, Zürich, Switzerland. E-mail: cristina.nevado@chem.uzh.ch; Fax: (+41) 446353948; Tel: (+41) 446353945*
[b] *Department of Biochemistry, University of Zurich, Winterthurerstrasse 190, CH-8057, Zürich, Switzerland*
[c] *Institute of Oncology Research, Faculty of Biomedical Sciences, USI, Bellinzona, Switzerland*
[d] *Department of Pharmacy, University of Munich, Butenandstrasse 5-13, 81377 Munich, Germany*
[e] *SIB Swiss Institute of Bioinformatics, Lausanne, Switzerland*
[f] *Oncology Institute of Southern Switzerland (IOSI), Bellinzona, Switzerland*

† Electronic supplementary information (ESI) available: General procedures for the synthesis, characterization and biological evaluation of all reported compounds can be found in the ESI. See DOI: 10.1039/d0md00049c

Design of new type II quinoxaline inhibitors

Within our first generation of quinoxaline EphB4 inhibitors (including type I, $I_{1/2}$ and II),[8d] compound **1** proved to be the most potent type $I_{1/2}$ ligand *in vitro* inducing a cytostatic effect in an *in vivo* cancer model. Interestingly, compound **2** represents a type II inhibitor bearing a urea linker that offers an interesting anti-proliferative profile over a cell cancer panel (Fig. 1).[8d]

The type II binding mode with the Asp-Phe-Gly (DFG)-out conformation of the kinase was confirmed by X-ray diffraction analysis of the catalytic domain of EphA3 in complex with **2** (Fig. 2A, PDB code 4P5Z).[8d] The pyrrolo[3,2-*b*]quinoxaline scaffold occupies the ATP binding site with the phenyl substituent located in the hydrophobic pocket that is generated when the kinase adopts an inactive DFG-out conformation. Compound **2** is able to form four hydrogen bonds within the hinge region of the kinase *via* the amino and amide substituents of the pyrrole ring: the amino substituent at position 2 is involved in a bifurcated hydrogen bond with the side chain hydroxyl of the Thr693 gatekeeper and the backbone carbonyl of Glu694, whereas the amide substituent at position 3 forms two hydrogen bonds with the backbone polar groups of Met696. In addition, the urea linker establishes three extra hydrogen bonds acting as a hydrogen bond acceptor from the Ser757 side chain and the amide backbone of Asp758, and hydrogen bond donor to the side chain of Glu664. The m-CF_3-phenyl moiety is located in the hydrophobic pocket originating from the displacement of the Phe765 side chain of the DFG motif in the DFG-out conformation of the kinase.

We have also solved the X-ray structure of the clinical candidate BIRB796 (**3**) in complex with the catalytic domain of EphA3 (Fig. 2B, PDB code 4TWN).[11] Compound **3** is a selective p38 MAP kinase inhibitor developed by Boehringer Ingelheim for the treatment of rheumatoid arthritis and other inflammatory conditions including Crohn's disease and psoriasis that has undergone several clinical trials.[3a,12] Compound **3** is a type II kinase inhibitor that is characterized by a pyrazole ring bearing a *tert*-butyl substituent nested within the hydrophobic pocket. Similar to our type II inhibitor **2**, the urea linker in inhibitor **3** establishes a hydrogen bond network with Asp758 and Glu664. This structure inspired further modifications of compound **1**. In particular, the superposition of compounds **2** and **3** reveals an overall similar binding mode and a clear overlap of the urea linker and its substituents (Fig. 2C), which prompted us to introduce a *tert*-butyl substituted pyrazole scaffold within our quinoxaline inhibitors series. We decided to synthesize not only the 4-methyl phenyl substituted pyrazole ring present in compound **3**, but also a quinoline substituted one mimicking compound DCC-2036 (**4**),[13] a BCR-ABL1 inhibitor that underwent clinical trials for the treatment of chronic myeloid leukemia (Fig. 2D).[14]

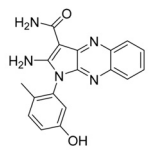

1

$\Delta T_m = 11.2$ °C
$EC_{50} = 5.4$ nM
GI_{50} (K562) = 229 nM

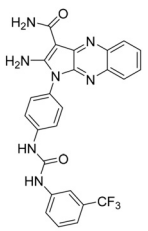

2

$\Delta T_m = 14.3$ °C
$EC_{50} = 89$ nM
GI_{50} (K562) = 3920 nM

Fig. 1 2D structures of previously developed type $I_{1/2}$ and II quinoxaline inhibitors **1** and **2**.[8d] EC_{50} values were measured in a cellular phosphorylation assay using mouse embryonic fibroblasts (MEF) that overexpress EphB4. ΔT_m values have been determined using differential scanning fluorimetry assay.

Synthesis of new type II quinoxaline inhibitors

The synthesis of the novel type II quinoxaline derivatives bearing the *tert*-butyl pyrazole moiety is shown in Scheme 1. Compound **5** was prepared according to previously reported procedures by condensation of commercially available 2,3-dichloroquinoxaline with malononitrile in the presence of sodium hydride.[15] The substitution of the chlorine at position 3 with synthetically prepared anilines **6a**, **b** (ref. 16) followed by cyclization afforded intermediates **7a**, **b** (ref. 17) (Scheme 1), which were then hydrolyzed under strong acidic conditions affording the final compounds **8a**, **b**.

Potency assessment: differential scanning fluorimetry and EC_{50} determination

The binding of the two novel type II quinoxaline inhibitors **8a**, **b** towards the tyrosine kinases EphA3 and EphB4 was first studied *in vitro* and compared to our first generation quinoxaline inhibitors **1** and **2**.[8d] Differential scanning fluorimetry (DSF) was used to measure the increase in thermal stability of EphA3 upon ligand binding.[18] Compounds **1** and **2** exhibited pronounced thermal shifts of 11.2 and 14.3 °C respectively, while the new inhibitors **8a**, **b** showed even higher values (17.3 and 19.3 °C respectively, Table 1). However, when compounds **8a**, **b** were then tested in cellular phosphorylation assays on MEF cells transfected with Myc-tagged human EphB4, their potency dropped compared to initial compound series to EC_{50} values of 360 and 1100 nM, respectively (Table 1).

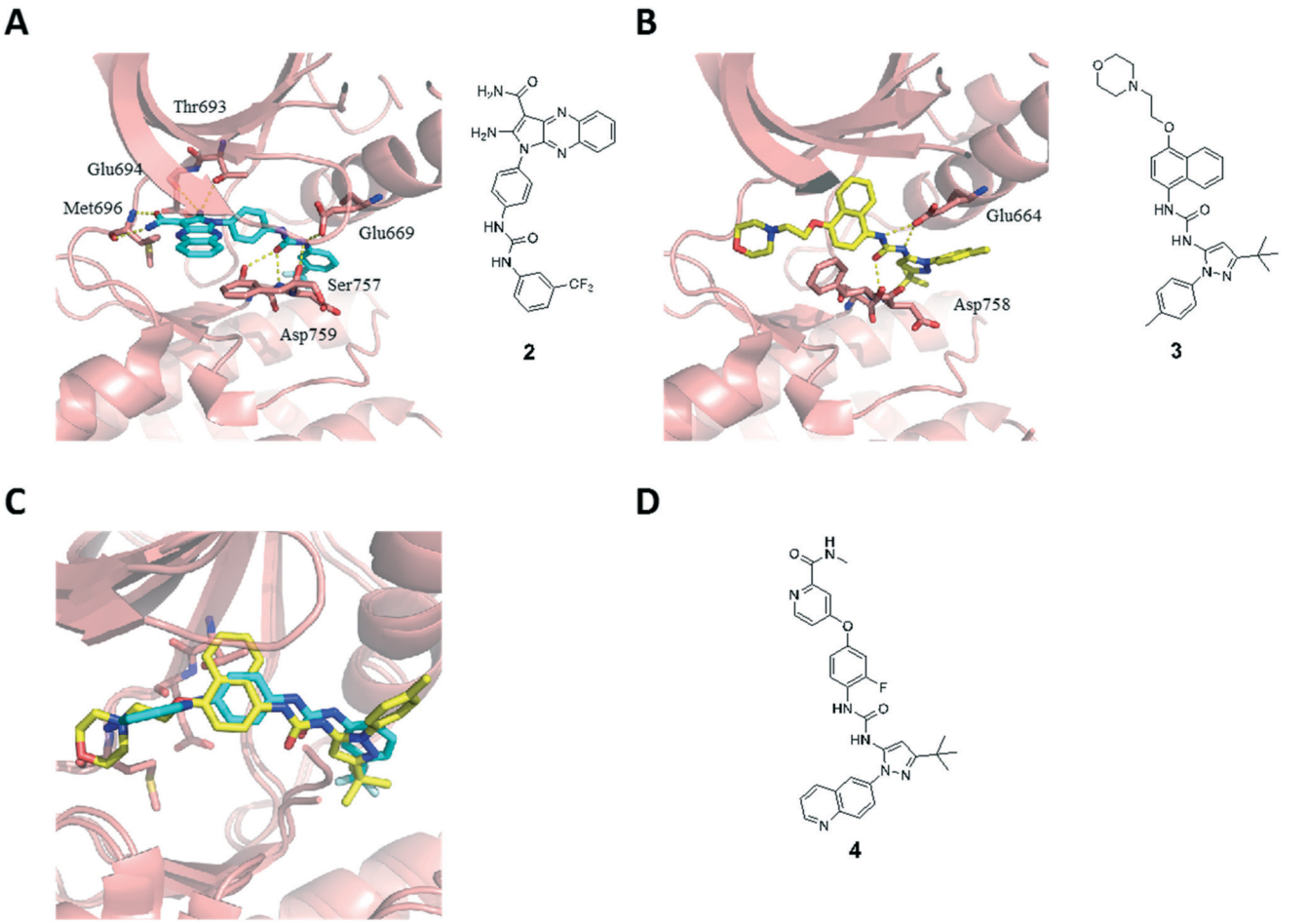

Fig. 2 Crystal structures of the catalytic domain of the tyrosine kinase EphA3 in complex with the low-nanomolar inhibitors **2** (A) and **3** (B) and superposition of the two inhibitors **2** and **3** (C). The ATP binding site of the EphA3 kinase is shown in pink ribbons while the side chains mentioned in the text and the inhibitors are shown by sticks in blue and yellow for compounds **2** and **3**, respectively. (D) 2D structure of the BCR-ABL1 inhibitor DCC-2036 (**4**).

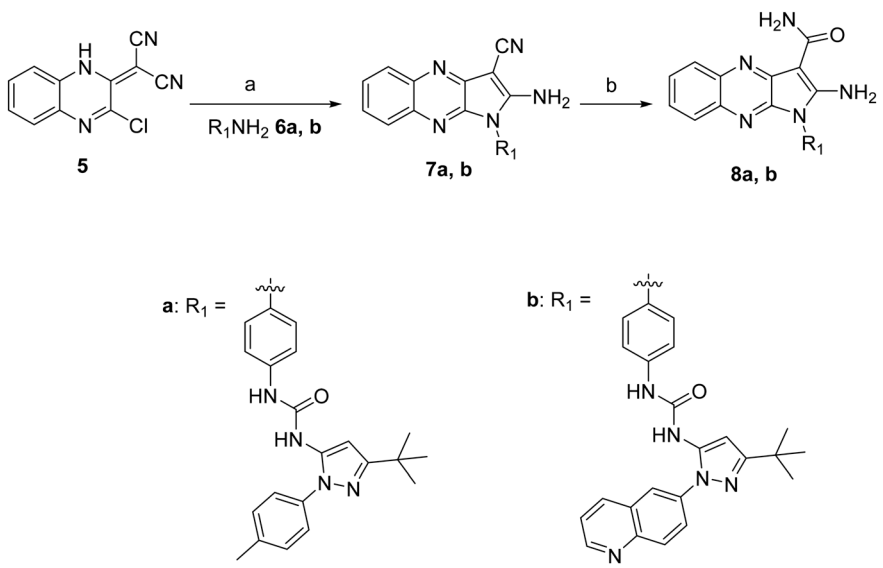

Scheme 1 Reagents and reaction conditions: a) **6a**, **b** (1.2 equiv.), DMF, 80 °C, 12 h, 55–62%. b) H_2SO_4, 25 °C, 30 min, 89–90%.

Table 1 EphA3/EphB4 inhibition data for the synthesized quinoxaline derivatives

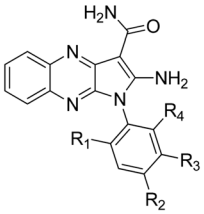

Compound	Type of binding	R_1	R_2	R_3	R_4	Thermal shift (°C)[a]	Cellular EC_{50}[b] (nM)
1	$I_{1/2}$	Me	H	OH	H	11.2	5.4
2	II	H	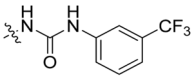	H	H	14.3	89
8a	II	H	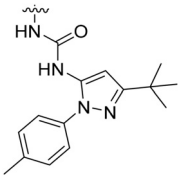	H	H	17.3	360
8b	II	H	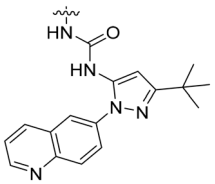	H	H	19.3	1100

[a] Average values of triplicate measurements. The standard deviation is smaller than 0.5 °C. [b] Cellular EC_{50} values were measured in a cellular phosphorylation assay using MEF cells overexpressing EphB4 at Proqinase.

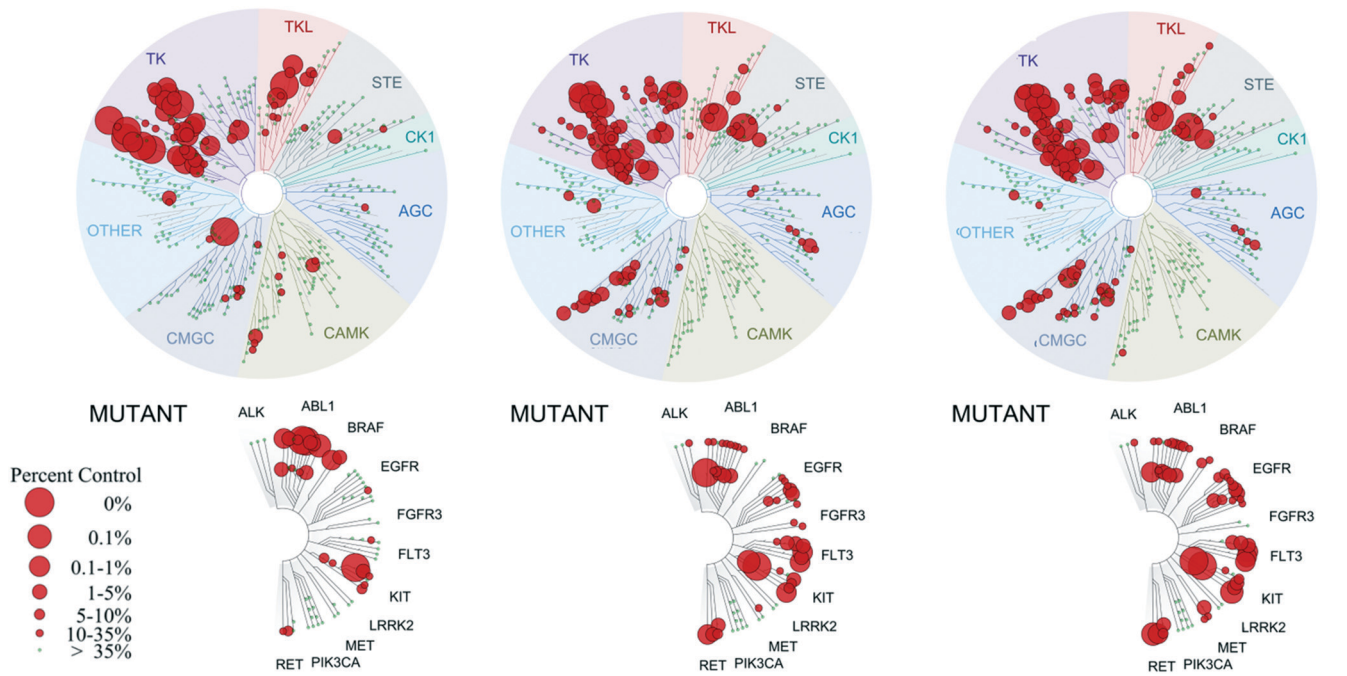

Fig. 3 Selectivity profiles of compound **1** (left), **8a** (center) and **8b** (right) tested on a panel of 453 protein kinases at DiscoveRx. Measurements were performed at a concentration of 1 μM of the inhibitor. The affinity is defined with respect to a DMSO control. The dendrogram was obtained from KinomeScan using the KinomeTree software.[19]

Selectivity profiles from biochemical assays

Given the potency loss observed towards EphB4 in the cell based assays for compounds **8a**, **b** (Table 1), we decided to assess the influence of the new urea substituents on the selectivity over a broad panel of kinases. The selectivity profile was obtained by an *in vitro* competition binding assay that reports on binding affinity with no ATP required, using recombinant kinases (KINOMEscan at DiscoveRx).[19] The selectivity panel consisted of 453 human kinases, 58 of which were disease related mutant kinases (mainly of ABL1, EGFR, and PIK3CA). Single dose measurements were carried out at 1 μM concentration of the ligand.

Compounds **8a** and **8b** present a very similar selectivity profile that differs from that obtained for compound **1** (Fig. 3). Quantitatively, 60 kinases (14 of which are disease-related mutants) are more strongly inhibited by compounds **8a**, **b**, where the difference between the affinity of **8a** or **8b** and compound **1** is at least 60% (expressed as% with respect to DMSO control). A total of 31 out of the 46 non-mutant kinases are serine/threonine-specific protein kinases, more than half of them belonging to the CMGC kinase family, and several are CDK kinases, which are involved in critical cellular processes.[20] This data clearly suggests a broader selectivity profile for compounds **8a**, **b**, which are also able to inhibit clinically relevant mutant kinases including ABL1, EGFR, FLT3, KIT, and MET. Interestingly, the activity towards EphB2, 3 and 4 kinases drops significantly in compounds **8a**, **b**, in line with the EC_{50} values obtained in cells overexpressing EphB4 (Table 1).

Anti-proliferative activity and gene expression profiling

Compounds **8a** and **8b** were screened against the NCI-60 cancer cell line panel and compared to our previously developed quinoxalines (**1**, **2**) and FDA-approved kinase inhibitors dasatinib and imatinib (Fig. 4). The two compounds presented a broader anti-proliferative activity than compounds **1** and **2** (which is in line with their broader selectivity profiles) and a significant correlation in terms of GI_{50} values across the different cell lines. The leukemia K-562 cell line was particularly sensitive towards the two optimized type II quinoxaline inhibitors, showing remarkably good GI_{50} values (31 and <10 nM, respectively).

In an effort to understand the mode of action of our quinoxaline inhibitors, we compared the transcriptome of K562 cells (one of the most sensitive cell lines towards our compounds, Fig. 4) after 6 hours of exposure to DMSO, as vehicle, to 1 μM of compound **8b** or 1 μM of dasatinib, for reference (ESI† – RNA-Sequencing Table). Compound **8b** and dasatinib caused very similar changes in the transcriptome of the cells (Fig. 5A). Compound **8b** downregulated MYC and E2F targets, genes known to be involved in oxidative phosphorylation, unfolded protein response, proteasome pathway, PI3K/AKT/mTOR signaling, spliceosome and DNA repair (ESI† – RNA-Seq Table compound **8b**). In contrast, genes negatively regulated by RAS were enriched among the transcripts upregulated by compound **8b** (Fig. 5B). The gene expression signature of compound **8b** overlapped with that of dasatinib on tumor infiltrating macrophages, and with PI3K/mTOR inhibitors in different tumor models (Fig. 5B) (ESI† – RNA-Seq Table compound **8b**). Same signatures were observed in dasatinib treated cells (ESI† – RNA-Seq Table dasatinib).

Chemical proteomics

We decided to perform a chemical proteomics experiment on our best quinoxaline inhibitor **8a** aiming to obtain the global proteomic profiles of this molecule in an unbiased cellular setting. This approach required the synthesis of a tethered inhibitor containing a suitable functional group that would

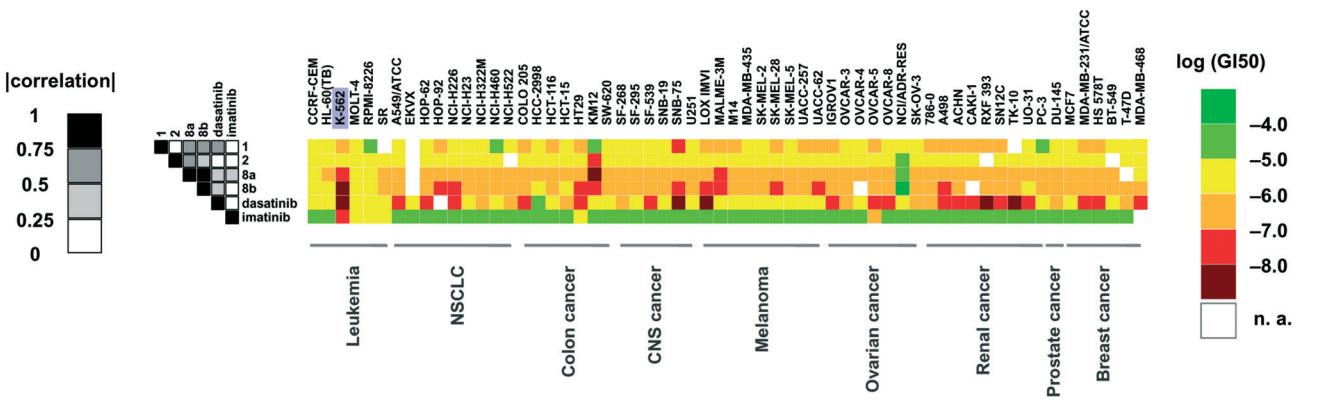

Fig. 4 The antiproliferative activity of quinoxalines **1**, **2**, **8a** and **8b** is shown together with the growth inhibition of two FDA approved anticancer drugs (dasatinib and imatinib) evaluated on the NCI-60 cancer cell line panel. The growth inhibition is shown as a matrix with cell lines and compounds arranged horizontally and vertically, respectively. The legend bar shows the color coding, which reflects the log(GI_{50}) value, with red and green indicating high and low toxicity, respectively. The grey scale on the left hand side of the figure shows the absolute value of the correlation of the compounds' GI_{50} values over for the different cell lines.

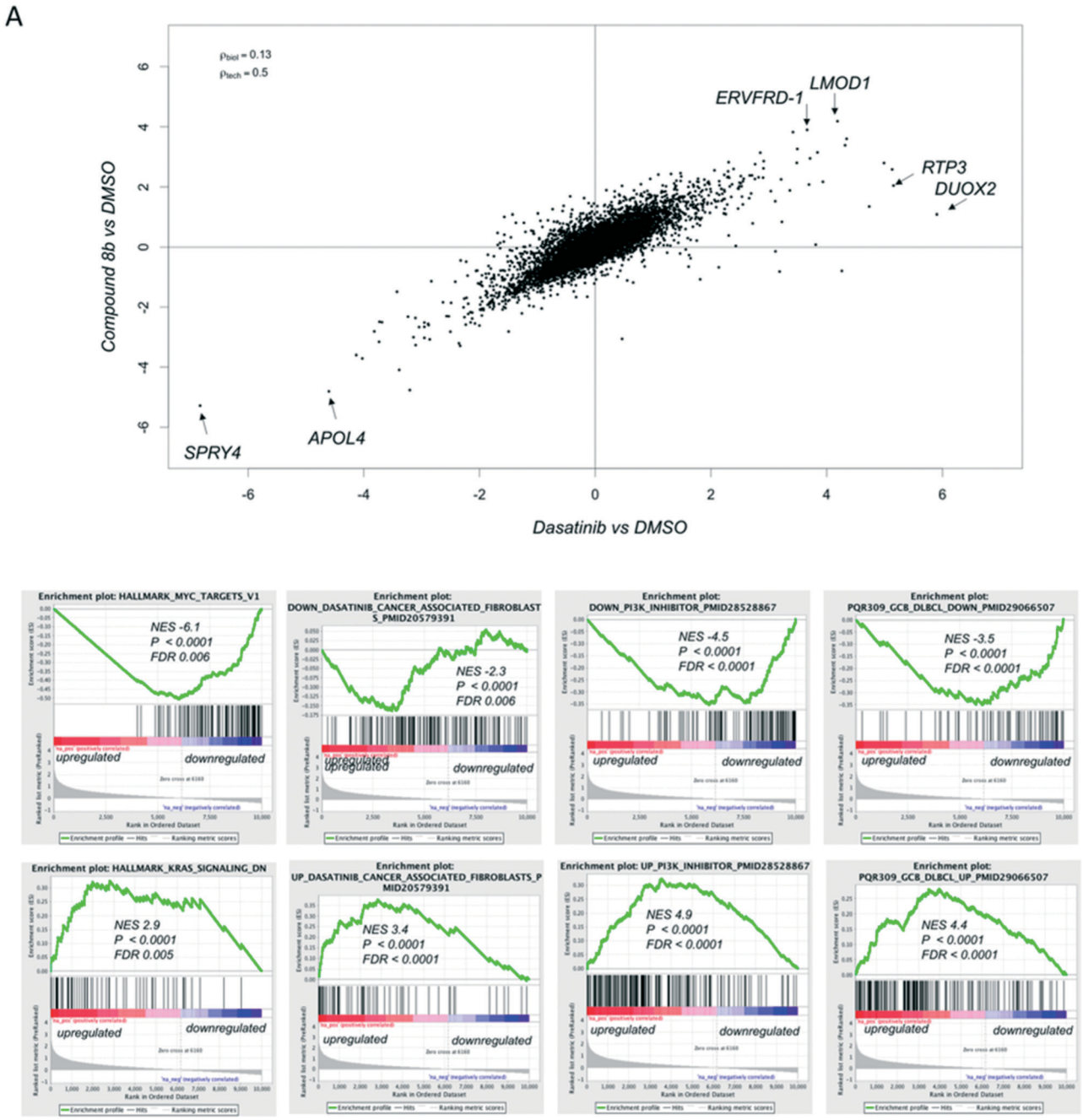

Fig. 5 Transcriptome analysis of CML K562 cells exposed to compounds **8b** or to dasatinib. (A) Scatter plots by log 2 fold gene expression changes in compound **8b**/DMSO-treated K652 *vs.* dasatinib/DMSO-treated K562 cells. (B) Representative GSEA plots illustrating the transcriptional expression signature enrichment in genes downregulated (upper panel) and upregulated (lower panel) after exposure to DMSO or compound **8b** in K562 cells. Green line represents the enrichment score; bars in the middle portion of the plots show where the members of the gene set appear in the ranked list of genes; positive or negative ranking metric indicate respectively correlation or inverse correlation with the profile; FDR, false discovery rate; *P*, probability value; NES, normalized enrichment score.

allow the attachment to a resin in a covalent fashion. Based on the X-ray structure of compound **2** (Fig. 2A) we envisioned that the introduction of a linker at the 7 position of the quinoxaline moiety would be tolerated due to its solvent accessibility. Thus, the analogue of compound **8a**, bearing a primary amino group suitable for immobilization, was synthesized, affording compound **13** (Scheme 2).

Intermediate **9** was prepared in three steps as previously reported starting from the commercially available 4-nitrobenzene-1,2-diamine.[15b,21] The substitution of the chlorine at position 3 with synthetically prepared aniline **6a** (ref. 16) followed by cyclization in DMF at 80 °C afforded intermediate **10**.[17] The nitro group was reduced in the presence of Pd on activated charcoal and a hydrogen

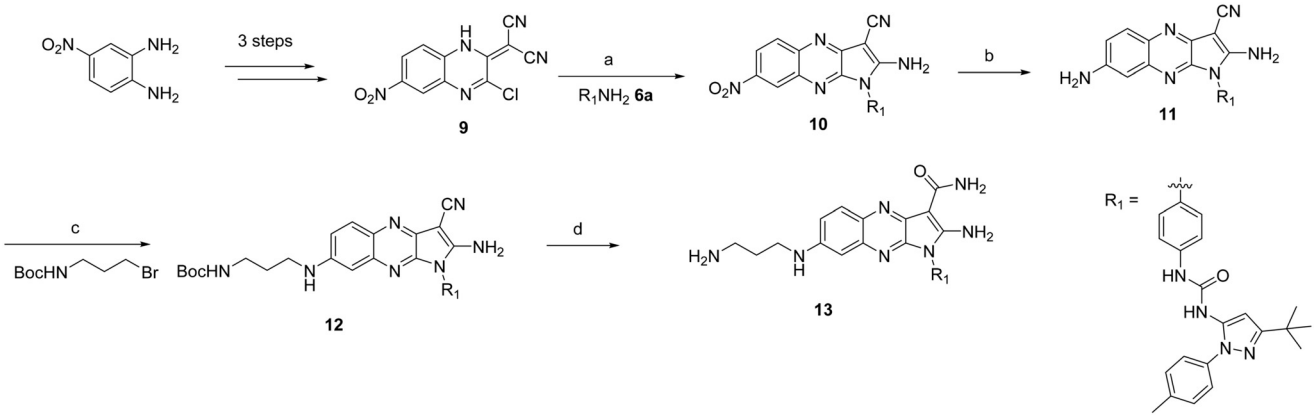

Scheme 2 Reagents and reaction conditions: a) **6a**, DMF, 80 °C, 4.5 h, 71%. b) H_2, Pd/C, MeOH, rt, 4 h, 70%. c) *tert*-Butyl (3-bromopropyl)carbamate, KI, DIPEA, DMF, 80 °C, 6 h, 29%. d) H_2SO_4, 25 °C, 30 min, quantitative yield.

atmosphere yielding the desired aniline **11** in good yield, which was further reacted with *tert*-butyl (3-bromopropyl)-carbamate to yield intermediate **12**. In the final step, strong acidic conditions were employed resulting in the hydrolysis of the nitrile group and removal of the Boc protecting group in quantitative yield, affording the intermediate **13**.

The inhibitory activity of **13** was then compared to its parent compound **8a** by measuring the ABL2 kinase activity in a competition binding assay (Fig. 6).[19] Crucially, no activity loss was observed for compound **13**, making it a suitable probe for our chemical proteomics study. More importantly, the selectivity profile of compound **13** linearly correlates to its parent compound **8a** as determined at 1 μM concentration in a panel of 453 kinases with an R^2 value of 0.8 (Fig. 6C) by a competition assay.[19]

The tethered analogue **13** was covalently bound to agarose polymer beads and incubated with the cell lysate of K562 leukemia cells (beads treated with DMSO were used as control). The beads were subsequently loaded onto spin columns, washed, and the protein binders were eluted with formic acid as previously reported.[5b] Among the 250 proteins identified by MS analysis as pulled down with immobilized compound **13** (Table S1†), there were 16 kinases (Table 2), five of which turned out also as targets in the selectivity profile analysis (LYN, BTK, YES, CSK and ABL2), plus PRKDC, MTOR, AGK, PI4KA (Table 2).

Four of the major interactors of quinoxaline **13**, LYN, BTK, CSK and YES1, are nanomolar binders already identified in the *in vitro* selectivity profile (Fig. 3). LYN, YES1, BTK and CSK are inhibited to 0.5, 1.9, 3.3 and 0.65% control respectively by our small molecule **13** (0.85, 9.6, 0.95 and 0.9% control, by the parent compound **8a** respectively) at 1 μM concentration. The 250 human proteins belonged to pathways related to protein secretion, oxidative phosphorylation, DNA repair, MYC and E2F targets, IL6/JAK/STAT3 signaling, glycolysis, mitotic spindle, and mTORC1 signaling.

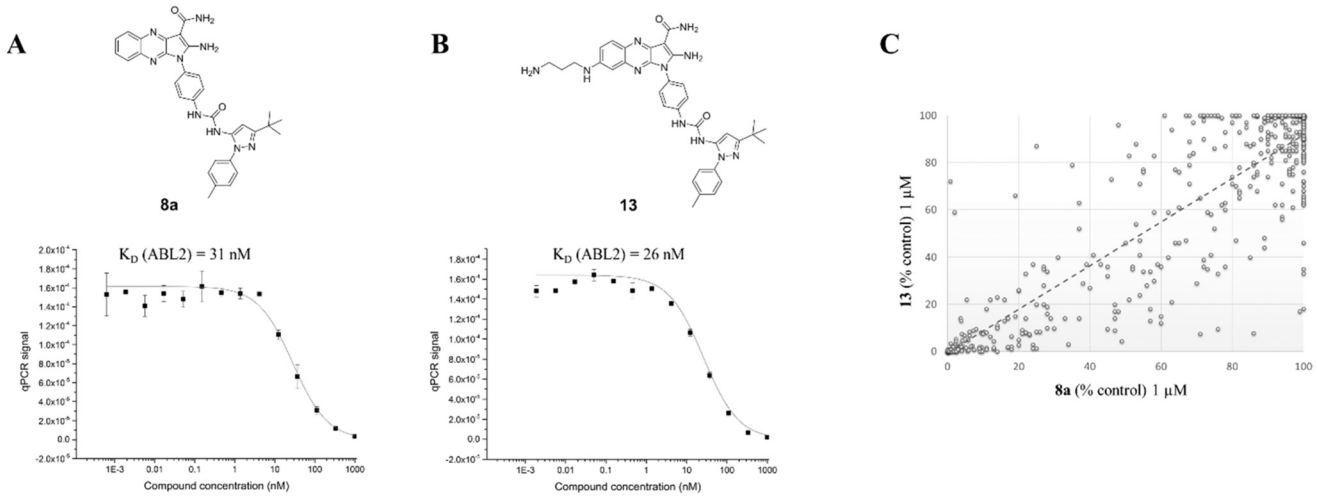

Fig. 6 (A and B) *In vitro* inhibitory activity towards ABL2 kinase of compounds **8a** and **13**. (C) Probe compound **13** and its parent compound **8a** show a strong correlation across a 453 kinase panel at 1 μM concentration, demonstrating the validity of compound **13** as a probe for chemical proteomic studies.

Table 2 Kinases identified in the pull down assay with compound **13** as bait

Gene name	Description	Fold change[a]
PRKDC	DNA-dependent protein kinase catalytic subunit	6172
LYN	Tyrosine-protein kinase Lyn	1721
ERLIN2	Erlin-2	1620
YES1	Tyrosine-protein kinase yes	1020
BTK	Tyrosine-protein kinase BTK	1216
MTOR	Serine/threonine-protein kinase mTOR	1116
CSK	Tyrosine-protein kinase CSK	1115
AGK	Acylglycerol kinase, mitochondrial	912
CDK1	Cyclin-dependent kinase 1	6.6
NDKA	Nucleoside diphosphate kinase A	6
GLPK	Glycerol kinase	5.5
ABL2	Abelson tyrosine-protein kinase 2	5
PDXK	Pyridoxal kinase	5
NDKB	Nucleoside diphosphate kinase B	5
PI4KA	Phosphatidylinositol 4-kinase alpha	5
SQSTM1	Sequestosome-1	5

[a] The peptide count average of the two duplicate measurements is given.

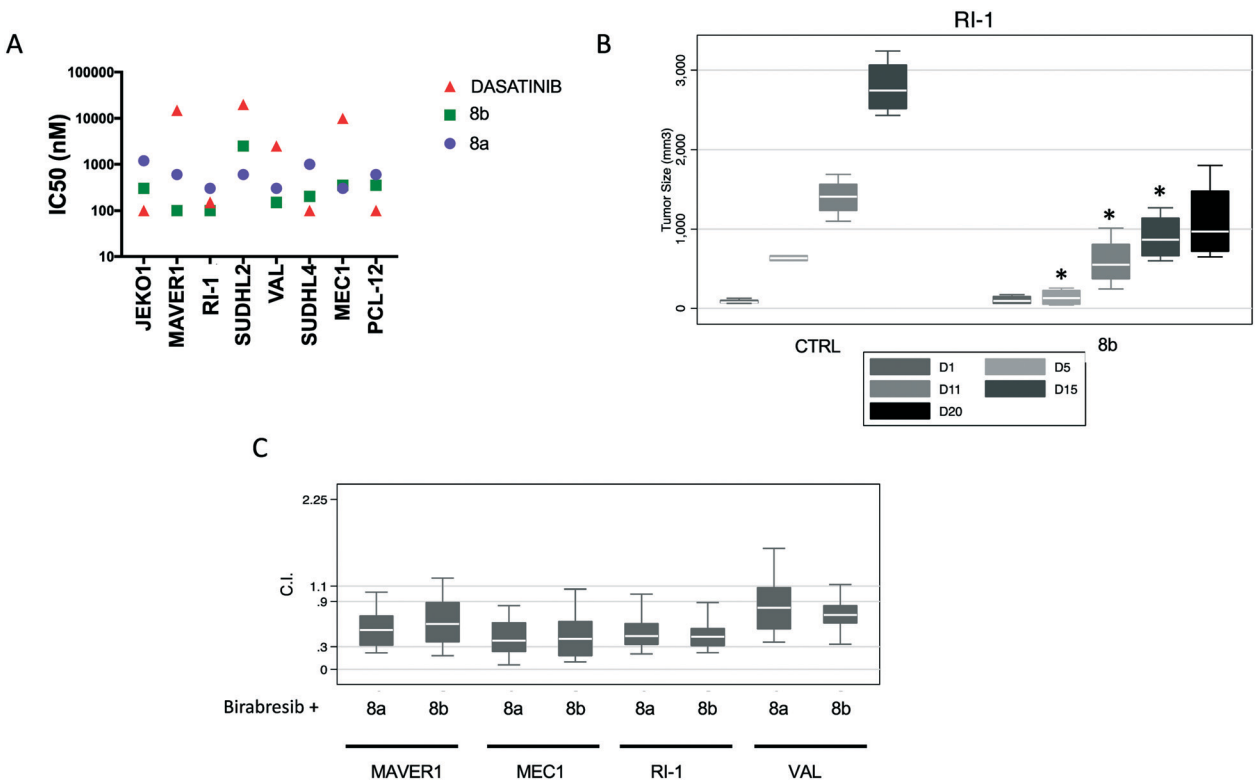

Fig. 7 Anti-tumor activity of compounds **8a** and **8b** in lymphoma models. (A) Eight B-cell lymphoma cell lines derived from mantle cell lymphoma (MCL) (Jeko1, MAVER1), chronic lymphocytic leukemia (MEC-1, PCL-12) and diffuse large B cell lymphoma (DLBCL) of the activated B cell like (ABC) (RI-1, SU-DHL-2) or of the germinal center B cell (GCB) (VAL, SU-DHL-4) were exposed to increased concentration of **8b** or **8a** for 72 h. (B) Effects of **8b** in a xenograft model of ABC-DLBCL. NOD-Scid mice subcutaneously inoculated with RI-1 cells (15 × 10 (ref. 6)) were split in three groups respectively treated with **8a** (100 mg kg^{-1}, IP, n = 4, data not shown), **8b** (100 mg kg^{-1}, IP, n = 4) and control vehicle (n = 4). Y-Axis, tumor volume in mm^3. X-Axis, days (D) of treatment. For compound **8b** *vs.* CTRL, D5-D15, $p < 0.05$. In each box-plot, the line in the middle of the box represents the median and the box extends from the 25th to the 75th percentile (interquartile range, IQ); the whiskers extend to the upper and lower adjacent values (*i.e.*, ±1.5 IQ); outside values have been omitted from the figure. (C) Values of the combination index (C.I.) of **8a** or **8b** with birabresib in ABC-DLBCL and MCL cell lines.

Inhibitors 8a and 8b in preclinical models of lymphoma

The engagement of target kinases LYN, BTK and mTOR by quinoxaline inhibitors demonstrated by the proteomics data prompted the investigation of their activity against lymphomas (not included in the NCI-60 panel), for which these three kinases are highly relevant. Anti-proliferative activity of **8a** and **8b** was assessed, in parallel to dasatinib, in eight B-cell lymphoma cell lines derived from mantle cell lymphoma (MCL) (Jeko1, MAVER1), chronic lymphocytic leukemia (MEC-1, PCL-12) and diffuse large B cell lymphoma (DLBCL) of the activated B cell like (ABC) (RI-1, SU-DHL-2) or of the germinal center B cell (GCB) (VAL, SU-DHL-4). Compounds were active with median GI_{50} of 600 nM (95% C. I. 300–1065 nM) and 250 nM (95% C.I. 100–1049 nM), respectively and their anti-tumor activity appeared more potent than dasatinib (median IC_{50} = 1325 nM, 95% C.I. 100–16 625 nM), in particular in four of the cell lines (MAVER1, SU-DHL-2, VAL and MEC1) (Fig. 7A).

The anti-lymphoma activity of compounds **8a** and **8b** was then assessed using a mouse xenograft model with the ABC DLBCL RI-1 cell line. Compound **8a** turned out to be very toxic already after the first dose, due to swelling of the area surrounding the injection and body-weight loss, and had to be stopped although the body weight started to recover after two weeks without treatment. Inhibitor **8b** was administered once every 5 days and was well tolerated with no general toxicity or body-weight loss. After two weeks of treatment, xenografts treated with **8b** were three times smaller than the control group or than the group treated with the initial single dose of **8a** at the end of the experiment (day 15) (Fig. 7B).

Dasatinib as well as inhibitors of BTK or mTOR are synergistic when combined with BET bromodomain inhibitors.[22] Thus, we combined compounds **8a** and **8b** with birabresib (MK-8628/OTX015), a BET bromodomain inhibitor with preclinical and early clinical anti-lymphoma activity.[22b,23] Synergism, *i.e.*, combination index (CI) values smaller than 1.0, was observed with the combination of compound **8a** or **8b** with birabresib in all the four cell lines that were studied (Fig. 7C).

Cellular angiogenesis assay

The implication of numerous kinases in angiogenesis[24] led us to examine the efficacy of our inhibitors on tube formation *via* an *in vitro* matrigel angiogenesis assay. Angiogenesis, the process of vascular growth by sprouting from pre-existing vessels, is a key player during tumor growth and metastasis in the context of several diseases including cancer, macular degeneration, diabetic retinopathy and arthritis.[3a] A remarkable effect was observed for the novel quinoxaline **8a** (65, 90, and 100% inhibition of tube length, total branching points and total loops respectively, Fig. 8) in comparison to our previously developed inhibitors **1** (9, 23 and 21% inhibition of tube length, total branching points and total loops respectively) and **2** (5, 9 and 13% respectively).[9] We hypothesize that the promising angiogenesis inhibition results obtained for compound **8a** could be due to its ability to inhibit several CDK kinases (in contrast to compound **1**, Fig. 3), as CDK inhibitors have been reported to block angiogenesis *in vitro* and *in vivo*.[25] Further, these results are in line with those previously reported for dasatinib and related TKI inhibitors.[26]

Conclusions

Two quinoxaline-containing chimeric kinase inhibitors **8a** and **8b** were designed based on the available X-ray structures of EphA3-inhibitor complexes through compound merging. They inhibit mainly tyrosine kinases and show broader spectrum of activity than the parent compound **1**, as well as high anti-proliferative activity against several cancer cell lines, as demonstrated in the NCI-60 cell line panel screening. Immortalised myelogenous leukemia cell line K562 was shown to be particularly sensitive and was selected for further investigations to elucidate the mode of action of compounds **8a–b**. Transcriptomic profiling revealed orthogonal effects of compounds **1** and **8b** on gene expression, with the latter closely resembling the effect profile of dasatinib, the SRC-family protein tyrosine kinase inhibitor. By conducting a chemical proteomics study we identified 17 kinases as potential binders of compounds **8a**,

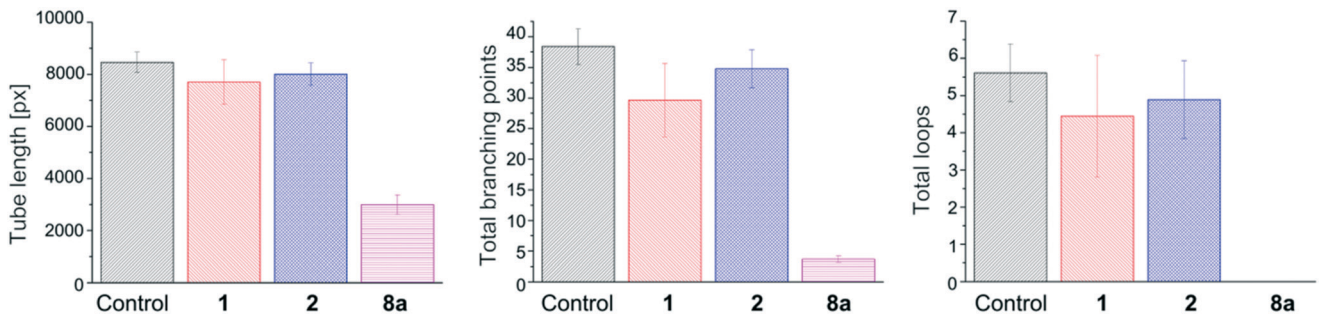

Fig. 8 *In vitro* angiogenesis assay on tube formation. Compounds were incubated with human umbilical vein endothelial cells (HUVEC) cells seeded on matrigel for 15 h. Tube length (left), total branching points (middle) and total loops (right) were quantified. All measurements were done at least in triplicate, and their SEM values are indicated as error bars.

including the known dasatinib targets LYN, BTK, CSK and YES1. Together, these studies have inspired two possible applications of the developed chimeric compounds. Demonstrated ability of our inhibitors to inhibit the CDKs prompted us to investigate effect of compound **8a** on inhibiting angiogenesis *in vitro*, showing remarkable improvement compared to the parent compound **1**. In turn, their engagement with the kinases LYN, BTK and mTOR, which are relevant in lymphomas, triggered *in vitro* and *in vivo* studies on compound **8a–b** in various lymphoma models. Both compounds have shown submicromolar IC_{50} values in five lymphoma cell lines. A significant decrease in tumor size is observed in an RI-1 lymphoma xenograft mouse model at a dose of 100 mg kg^{-1} of compound **8b**, without any associated mean body weight loss. These results indicate promise for therapeutic use of developed inhibitors *in vivo*. Further evaluation of compound **8b** in a xenograft mice model established with a more responsive cell line than the RI-1, such as the K562 human chronic myeloid leukemia cell line, might demonstrate even greater extent of tumor size control.

Accession codes

PDB codes for EphA3 in complex with the inhibitors **2** and **3** are 4P5Z and 4TWN, respectively.

Author contributions

CN, AC, FB and SZ conceived and designed the experiments. Experimental work was conducted by AU, CJ-T, DS, EG, CT, JD, JL, EB, GS, LC and PS. Crystallographic and computational work was conducted by PS, HZ and JD. The manuscript was written and edited by CN, AC, FB, PS, AU. CJ-T and EG.

Ethical statement

Mice maintenance and animal experiments were performed under institutional guidelines established for the Animal Facility at The Institute of Research in Biomedicine (IRB, Bellinzona, CH). and with study protocols approved by the local Cantonal Veterinary Authority (No. TI-20-2015).

Abbreviations

Eph	Erythropoietin-producing human hepatocellular carcinoma receptor
DFG	Aspartate-phenylalanine-glycine
ATP	Adenosine triphosphate
SPR	Surface plasmon resonance
DMF	Dimethylformamide
TBTU	*N*,*N*,*N*′,*N*′-Tetramethyl-*O*-(benzotriazol-1-yl)uronium tetrafluoroborate
DIPEA	Diisoproylethylamine
DCM	Dichloromethane
THF	Tetrahydrofuran
HOBt	Hydroxybenzotriazole
EDC	*N*-(3-Dimethylaminopropyl)-*N*′-ethylcarbodiimide
FRET	Fluorescence-resonance energy transfer
Abl	Abelson murine leukemia viral oncogene homologue
EGFR	Epidermal growth factor receptor
DDR	Discoidin domain receptor
Lck	Lymphocyte-specific kinase
CDK	Cyclin dependent kinase
DMSO	Dimethyl sulfoxide
MEF	Mouse embryonic fibroblasts
VEGF	Vascular endothelial growth factor
HUVEC	Human umbilical vein endothelial cells
NCI	National Cancer Institute
DTP	Developmental Therapeutics Program
IP	Intraperitoneal

Conflicts of interest

There is no conflict of interest to declare.

Acknowledgements

We thank Dr. Erich Brunner for interesting discussions regarding the chemical proteomic experiments. We also acknowledge and thank the NIH/National Cancer Institute for *in vitro* and *in vivo* evaluations of compounds under the Developmental Therapeutics Program (DTP), and in particular Dr. Stephen L. White of the NIH/NCI Drug Synthesis & Chemistry Branch for information and discussions relating to the *in vivo* studies. The authors would like to thank the Swiss National Science Foundation and the Swiss Cancer League (Krebsliga) for financial support (to AC and CN) and the Gelu Foundation (to FB). PŚ is a recipient of UZH Entrepreneur Fellowship in Biotechnology.

References

1 R. E. Hubbard, *Mol. BioSyst.*, 2005, **1**, 391.
2 Editorial article: Mechanism matters, *Nat. Med.*, 2010, 16, 347, DOI: 10.1038/nm0410-347.
3 (*a*) J. Lamb, E. D. Crawford, D. Peck, J. W. Modell, I. C. Blat, M. J. Wrobel, J. Lerner, J. P. Brunet, A. Subramanian, K. N. Ross, M. Reich, H. Hieronymus, G. Wei, S. A. Armstrong, S. J. Haggarty, P. A. Clemons, R. Wei, S. A. Carr, E. S. Lander and T. R. Golub, *Science*, 2006, **313**, 1929; (*b*) J. Lamb, *Nat. Rev. Cancer*, 2007, **7**, 54.
4 U. Rix, O. Hantschel, G. Duernberger, L. L. R. Rix, M. Planyavsky, N. V. Fernbach, I. Kaupe, K. L. Bennett, P. Valent, J. Colinge, T. Kocher and G. Superti-Furga, *Blood*, 2007, **110**, 4055.
5 (*a*) L. L. R. Rix, U. Rix, J. Colinge, O. Hantschel, K. L. Bennett, T. Stranzl, A. Muller, C. Baumgartner, P. Valent, M. Augustin, J. H. Till and G. Superti-Furga, *Leukemia*, 2009, **23**, 477; (*b*) N. V. Fernbach, M. Planyavsky, A. Muller, F. P. Breitwieser, J. Colinge, U. Rix and K. L. Bennett, *J. Proteome Res.*, 2009, **8**, 4753.
6 (*a*) G. Manning, D. B. Whyte, R. Martinez, T. Hunter and S. Sudarsanam, *Science*, 2002, **298**, 1912; (*b*) P. Cohen, *Nat. Rev. Drug Discovery*, 2002, **1**, 309.

7 (*a*) R. Li and J. A. Stafford, *Kinase Inhibitor Drugs*, John Wiley & Sons, Inc., Hoboken, New Jersey, 2009; (*b*) J. Blanc, R. Geney and C. Menet, *Anti-Cancer Agents Med. Chem.*, 2013, **13**, 731; (*c*) A. Kontzias, A. Kotlyar, A. Laurence, P. Changelian and J. J. O'Shea, *Curr. Opin. Pharmacol.*, 2012, **12**, 464; (*d*) Z. O'Brien and M. F. Moghaddam, *Expert Opin. Drug Metab. Toxicol.*, 2013, **9**, 1597; (*e*) F. M. Ferguson and N. S. Gray, *Nat. Rev. Drug Discovery*, 2018, **17**, 353.

8 (*a*) K. Lafleur, D. Huang, T. Zhou, A. Caflisch and C. Nevado, *J. Med. Chem.*, 2009, **52**, 6433; (*b*) H. T. Zhao, J. Dong, K. Lafleur, C. Nevado and A. Caflisch, *ACS Med. Chem. Lett.*, 2012, **3**, 834; (*c*) K. Lafleur, J. Dong, D. Huang, A. Caflisch and C. Nevado, *J. Med. Chem.*, 2013, **56**, 84; (*d*) A. Unzue, J. Dong, K. Lafleur, H. T. Zhao, E. Frugier, A. Caflisch and C. Nevado, *J. Med. Chem.*, 2014, **57**, 6834; (*e*) M. Xu, A. Unzue, J. Dong, D. Spiliotopoulos, C. Nevado and A. Caflisch, *J. Med. Chem.*, 2016, **59**, 1340.

9 A. Unzue, K. Lafleur, H. Zhao, T. Zhou, J. Dong, P. Kolb, J. Liebl, S. Zahler, A. Caflisch and C. Nevado, *Eur. J. Med. Chem.*, 2016, **112**, 347.

10 M. Brave, V. Goodman, E. Kaminskas, A. Farrell, W. Timmer, S. Pope, R. Harapanhalli, H. Saber, D. Morse, J. Bullock, A. Men, C. Noory, R. Ramchandani, L. Kenna, B. Booth, J. Gobburu, X. Jiang, R. Sridhara, R. Justice and R. Pazdur, *Clin. Cancer Res.*, 2008, **14**, 352.

11 J. Dong, H. T. Zhao, T. Zhou, D. Spiliotopoulos, C. Rajendran, X. D. Li, D. Z. Huang and A. Caflisch, *ACS Med. Chem. Lett.*, 2015, **6**, 79.

12 (*a*) C. Pargellis, L. Tong, L. Churchill, P. F. Cirillo, T. Gilmore, A. G. Graham, P. M. Grob, E. R. Hickey, N. Moss, S. Pav and J. Regan, *Nat. Struct. Biol.*, 2002, **9**, 268; (*b*) J. Regan, S. Breitfelder, P. Cirillo, T. Gilmore, A. G. Graham, E. Hickey, B. Klaus, J. Madwed, M. Moriak, N. Moss, C. Pargellis, S. Pav, A. Proto, A. Swinamer, L. Tong and C. Torcellini, *J. Med. Chem.*, 2002, **45**, 2994.

13 W. W. Chan, S. C. Wise, M. D. Kaufman, Y. M. Ahn, C. L. Ensinger, T. Haack, M. M. Hood, J. Jones, J. W. Lord, W. P. Lu, D. Miller, W. C. Patt, B. D. Smith, P. A. Petillo, T. J. Rutkoski, H. Telikepalli, L. Vogeti, T. Yao, L. Chun, R. Clark, P. Evangelista, L. C. Gavrilescu, K. Lazarides, V. M. Zaleskas, L. J. Stewart, R. A. Van Etten and D. L. Flynn, *Cancer Cell*, 2011, **19**, 556.

14 https://clinicaltrials.gov/ was accessed on the 21st of March 2016.

15 (*a*) E. F. Pratt and J. Kereszte, *J. Org. Chem.*, 1967, **32**, 49; (*b*) C. A. Obafemi and W. Pfleiderer, *Molecules*, 2004, **9**, 223.

16 For further details see the ESI†.

17 H. Otomasu, S. Ohmiya, T. Sekuguch and H. Takahash, *Chem. Pharm. Bull.*, 1970, **18**, 2065.

18 F. H. Niesen, H. Berglund and M. Vedadi, *Nat. Protoc.*, 2007, **2**, 2212.

19 M. A. Fabian, W. H. Biggs, 3rd, D. K. Treiber, C. E. Atteridge, M. D. Azimioara, M. G. Benedetti, T. A. Carter, P. Ciceri, P. T. Edeen, M. Floyd, J. M. Ford, M. Galvin, J. L. Gerlach, R. M. Grotzfeld, S. Herrgard, D. E. Insko, M. A. Insko, A. G. Lai, J. M. Lelias, S. A. Mehta, Z. V. Milanov, A. M. Velasco, L. M. Wodicka, H. K. Patel, P. P. Zarrinkar and D. J. Lockhart, *Nat. Biotechnol.*, 2005, **23**, 329.

20 M. Malumbres, E. Harlow, T. Hunt, T. Hunter, J. M. Lahti, G. Manning, D. O. Morgan, L. H. Tsai and D. J. Wolgemuth, *Nat. Cell Biol.*, 2009, **11**, 1275.

21 J. Deng, E. Feng, S. Ma, Y. Zhang, X. Liu, H. Li, H. Huang, J. Zhu, W. Zhu, X. Shen, L. Miao, H. Liu, H. Jiang and J. Li, *J. Med. Chem.*, 2011, **54**, 4508.

22 (*a*) C. Xu, K. A. Buczkowski, Y. Zhang, H. Asahina, E. M. Beauchamp, H. Terai, Y. Y. Li, M. Meyerson, K. K. Wong and P. S. Hammerman, *Mol. Cancer Ther.*, 2015, **14**, 2382; (*b*) M. Boi, E. Gaudio, P. Bonetti, I. Kwee, E. Bernasconi, C. Tarantelli, A. Rinaldi, M. Testoni, L. Cascione, M. Ponzoni, A. A. Mensah, A. Stathis, G. Stussi, M. E. Riveiro, P. Herait, G. Inghirami, E. Cvitkovic, E. Zucca and F. Bertoni, *Clin. Cancer Res.*, 2015, **21**, 1628; (*c*) A. Stathis and F. Bertoni, *Cancer Discovery*, 2018, **8**, 24.

23 S. Amorim, A. Stathis, M. Gleeson, S. Iyengar, V. Magarotto, X. Leleu, F. Morschhauser, L. Karlin, F. Broussais, K. Rezai, P. Herait, C. Kahatt, F. Lokiec, G. Salles, T. Facon, A. Palumbo, D. Cunningham, E. Zucca and C. Thieblemont, *Lancet Haematol.*, 2016, **3**, e196.

24 (*a*) K. J. Gotink and H. M. W. Verheul, *Angiogenesis*, 2010, **13**, 1; (*b*) R. H. Adams, *Semin. Cell Dev. Biol.*, 2002, **13**, 55; (*c*) M. Jeltsch, V. M. Leppanen, P. Saharinen and K. Alitalo, *Cold Spring Harbor Perspect. Biol.*, 2013, 5.

25 (*a*) J. Liebl, V. Krystof, G. Vereb, L. Takacs, M. Strnad, P. Pechan, L. Havlicek, M. Zatloukal, R. Furst, A. M. Vollmar and S. Zahler, *Angiogenesis*, 2011, **14**, 281; (*b*) J. Liebl, S. B. Weitensteiner, G. Vereb, L. Takacs, R. Furst, A. M. Vollmar and S. Zahler, *J. Biol. Chem.*, 2010, **285**, 35932.

26 A. Gover-Proaktora, G. Granota, M. Pasmanik-Chor, O. Pasvolsky, S. Shapira, O. Raza, P. Raananic and A. Leader, *Leuk. Lymphoma*, 2018, **60**(1), 189.